



## Photodecolorization of Eriochrome Black T using NiS–P zeolite as a heterogeneous catalyst

Alireza Nezamzadeh Ejhieh<sup>a,b,\*</sup>, Mahshid Khorsandi<sup>a</sup>

<sup>a</sup> Department of Chemistry, Islamic Azad University, Shahreza Branch, P.O. Box 311-86145, Shahreza, Isfahan, Iran

<sup>b</sup> Razi Chemistry Research Center (RCRC), Islamic Azad University, Shahreza Branch, Iran

### ARTICLE INFO

#### Article history:

Received 18 June 2009

Received in revised form 20 October 2009

Accepted 13 November 2009

Available online 18 November 2009

#### Keywords:

Eriochrome Black T

NiS particles

Photodecolorization

Zeolite

### ABSTRACT

NiS–P zeolite was prepared by ion exchange and precipitation procedures and it was characterized by FT-IR, SEM and thermal methods. The prepared composite was used as a catalyst in the photodecolorization process of Eriochrome Black T (E.B.T.) dye in aqueous solution under UV irradiation. The effect of key operating parameters such as catalyst dosage, temperature, initial concentration of the dye and initial pH of the solutions were studied on the decolorization process of dye. The primary objective was to determine the optimal conditions for each of the parameters. UV–vis spectrophotometric measurements were performed for the determination of decolorization and mineralization extents. The optimal operation parameters were found as follows: pH 9.1, 0.8 g L<sup>-1</sup> of catalyst loading and 40 ppm of dye concentration. The NiS particles out of zeolite framework did not show significant decolorization efficiency. The decolorization process obeyed first-order kinetics.

© 2009 Elsevier B.V. All rights reserved.

### 1. Introduction

Nowadays, colors are inseparable elements of human daily life and they are used in almost all production sectors in industry. A little more than half of the total world dye production (700,000 tons per year) concentrates on textile dyes and some 15% are used for other substrates dyed in a similar manner to textiles (leather, paper, etc.) [1,2]. Fifteen percent of the total world production of dyes is lost during the dyeing process and is released in textile effluents [1,3]. The effluents from these industries causes the water bodies not only to become colored, but also causes environmental damage to living organisms by stopping the re-oxygenation capacity of water and also blocking sunlight, thereby, causing a disturbance in the natural growth activity of aquatic life. Furthermore, some of these dyes pass into drinking water and can cause damage to human life as some of these dyes are carcinogenic in nature. It is, therefore, essential to remove these dyes from water bodies or treat them in such a way so as to minimize the damage to the environment and also to decolorize the water [4–7]. Reactive azo dyes are the largest group of organic dyes with –N=N– group as a chromophore in the molecular structure. They represent more than a half of the global dye production especially because of their wide usage in dyeing industries due to the simple dyeing procedure [8,9].

This kind of effluent is also resistant to biological decolorization. Therefore, removal of such colored agents from aqueous effluents is a significant environmental importance.

There is currently a wide range of treatment technologies for these types of wastewater. Precipitation, ion exchange, solvent extraction, filtration and electrochemical treatment are the conventional methods for the removal of dyes from aqueous solutions [10–13]. All these methods have significant disadvantages such as incomplete ion removal, high-energy requirements and production of toxic sludge or other waste products that require further disposal. The efficiency and simplicity of advanced oxidation processes (AOPs) make them a suitable choice for the removal of toxic chemicals from wastewaters in the recent years [14–19]. Common AOPs involve Fenton and photo-Fenton processes, ozonation, electrochemical oxidation, photolysis with H<sub>2</sub>O<sub>2</sub> and O<sub>3</sub>, high-voltage electrical discharge process, TiO<sub>2</sub> photo-catalysis, radiolysis, water solution treatment by electronic or  $\gamma$  beams and various combinations of these methods [20,21]. Although common homogeneous Fenton systems offer a cost-effective source of hydroxyl radicals, there are some major drawbacks that limit the industrial applications of this technology: (i) the tight range of pH in which the reaction proceed, (ii) the need for recovering the precipitated catalyst after treatment and (iii) deactivation by some ion-complexing agents like phosphate anions. The resulting sludge may also contain organic substances as well as heavy metals and has to be treated further, thus increasing the overall costs [2].

Heterogeneous photo-catalysis is a branch of AOP where a semiconductor catalyst under UV irradiation is highly successful in the mineralization of pollutants. In heterogeneous photo-catalysis OH<sup>•</sup>

\* Corresponding author at: Department of Chemistry, Islamic Azad University, Shahreza Branch, P.O. Box 311-86145, Shahreza, Isfahan, Iran. Tel.: +98 321 3292073; fax: +98 321 3291018.

E-mail address: [arnezamzadeh@iaush.ac.ir](mailto:arnezamzadeh@iaush.ac.ir) (A.N. Ejhieh).

radicals are generated under UV irradiation of an aqueous solution which plays a major role in the decolorization of pollutants. In this method, redox reactions takes place on the surface of the semiconductor/solution interface upon irradiation of semiconductor particles with proper energy (wavelength) higher than the band gap of the catalyst. Due to absorption of proper energy/photons, the production of electron–hole pairs result on the surface of the catalyst which can reduce or oxidize different organic compounds in an aqueous solution. The oxidizing radicals formed upon reaction of holes with water could attack pollutant molecule and disintegrate it into  $\text{CO}_2$  and  $\text{H}_2\text{O}$  molecules which are non-toxic [22].

Among many semiconductors,  $\text{TiO}_2$  has been considered as one of the most promising photocatalyst [6]. However, poor adsorption, low surface area, absorption only a small fraction of sun light (2–3%), rapid recombination of electron–hole pair and difficulty of separation from solution properties lead to great limitations in exploiting the  $\text{TiO}_2$  to the best of its photoefficiency. Supported  $\text{TiO}_2$  is commonly reported to be less photoactive, due to the interaction of  $\text{TiO}_2$  with the support during the thermal treatments. Nonetheless, supporting with zeolites is found to be a better candidate as compared to other supporting materials. This is because normally zeolites have applications in many technological fields such as catalysis and wastewater treatment [6].

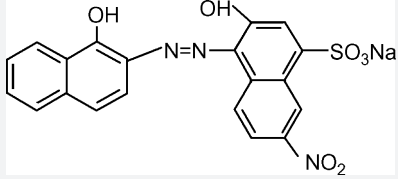
Zeolites modified with transition metal ions have received increasing attention as promising catalysts for a variety of important reactions [23]. Zeolites can serve as hosts to activate transition metal ions, offering a unique ligand system with multiple types of coordination for cations. In addition, the restricted pore size of zeolites could limit the growth or sintering of the nanoparticles of the cation even at high temperatures [24]. Zeolites are crystalline aluminosilicates with cavities, whose sizes can vary in the range from one to several tens of nanometers. It depends on the type of aluminosilicates framework, Si/Al ratio and origin of ion exchange cations, which stabilize negative charge of framework, etc [25].

Lewis acid sites are widely used in homogeneous catalysis to promote the reaction of organic substrate with oxidants. In the research area of green chemistry, development of new solid Lewis acids, active and selective for catalytic oxidation, is crucial especially on using environmentally benign oxidants. A significant step toward this goal is to identify the nature of Lewis acid sites, at the atomic level, existing in zeolites. Lewis acid sites can be attributed to extra framework aluminum species (EFAL) of octahedral or tetrahedral aluminum as well as tri-coordinated Al, partially dislodged in the framework. Zeolites are three-dimensional aluminosilicates containing exchangeable cations that act as Lewis acid sites. The framework oxygen atoms of alkali exchanged zeolites bear partial negative charge and behave as Lewis base. Zeolite P which was synthesized in this paper has a Si/Al ratio of 3.5 which is located in the range of 1–5 for zeolite P. By decreasing Si/Al ratio, zeolite P will load more NiS particles, which in turn causes an increase in photoreactivity of NiS–P catalyst.

The research subject of our group is the study on the effect of various transition metal sulfides incorporated in zeolites in photodecolorization of pollutants. In our knowledge, preparation of these sulfides, with respect to their oxides, is easy due to the large formation constant of these compounds. Low leaching of these sulfide compounds, due to low solubility, is another advantage. Sulfides of many transition metals show electronic and optical properties such as semiconductivity and photoconductivity. For example, nickel sulfide is a potential transformation toughening agent for semiconductor materials, while nickel disulfide adopts the pyrite structure and exhibits semiconducting properties. Thus, the synthesis of the 3d transition metal sulfides has attracted great interests for several decades [26].

In this work NiS formed inside the channels of zeolite P (channel size 3.9 Å), by precipitation after ion exchange process. The

**Table 1**  
Chemical structure and characteristics of E.B.T.

Chemical structure	
C.I. number	14,645
M.W.	461.38
$\lambda_{\text{max}}$ (nm)	526
pH (10 g L <sup>-1</sup> , H <sub>2</sub> O, 20 °C)	3.7
Sol. in water (20 °C)	50 g L <sup>-1</sup>
Sol. in ethanol (20 °C)	2 g L <sup>-1</sup>
Form	Solid
Color	Black

obtained composite is applied as photocatalyst in the decolorization of E.B.T. The effects of different parameters such as catalyst amount, initial concentration of the dye, initial pH and temperature of the dye solution were investigated on the decolorization efficiency of the dye. To our knowledge, this is the first study of NiS incorporated zeolites toward E.B.T. photodecolorization.

## 2. Experimental

### 2.1. Reagents

E.B.T. ( $\text{C}_{20}\text{H}_{12}\text{N}_3\text{NaO}_7\text{S}$ ) and all other chemicals with analytical grade were obtained from Merck. Double distilled-deionized water was used throughout the experiments. The pH of solutions was adjusted with sodium hydroxide or hydrochloric acid solution as appropriate. The main characteristics of E.B.T. are presented in Table 1.

### 2.2. Synthesis of zeolite P

Sodium silicate (acidimetric  $\text{Na}_2\text{O}$  7.5–8.5%, acidimetric  $\text{SiO}_2$  25.5–28.5%) and, aluminium chloride ( $\text{AlCl}_3 \cdot 6\text{H}_2\text{O}$ ) were used as silica and alumina sources, respectively. Sodium hydroxide (NaOH) and water were used as mineralizing agent and solvent, respectively. The NaOH solution (0.14 g/mL) was added to aluminate solution (0.165 g/mL) while the mixture was stirred and heated. Then, the aluminate solution was added slowly into 14.53 g of sodium silicate in the polyethylene bottle and aged at room temperature with stirring for 4 h. Finally, the mixture at pH 13 was transferred to a reactor inside an oven with temperature of 100 °C for 3 days. The solid product was filtered and washed with water until the pH of the filtrate dropped to 7. The products were dried at 100 °C for 24 h. The obtained sample was referred to as zeolite P.

### 2.3. Preparation of NiS/zeolite P

For ion exchange experiments, 8 g of zeolite P powder was added to 100 mL of 0.1 M  $\text{Ni}^{2+}$  solution (as nitrate salt) and stirred at room temperature for 8 h. The procedure was repeated twice to complete ion exchange. The sample was filtered off, washed with water and dried at 110 °C. The color of the obtained sample (Ni–P) was greenish blue. Finally, sulfurizing of the  $\text{Ni}^{2+}$  ion was carried out with 0.1 M  $\text{Na}_2\text{S}$  solution. To make the reaction with  $\text{S}^{2-}$  ions, 2 g of  $\text{Ni}^{2+}$ -exchanged zeolite was added to 100 mL of 0.1 M solution of  $\text{Na}_2\text{S}$  at a fixed temperature and stirred for 30 min. The obtained sample was washed with water and collected by filtration to completely remove the sulfide ions. The obtained sample was fine powder with pale grey color. The sample was kept at ambient conditions

and its color did not change during with time, indicating the high stability of the sample. To investigate the effect of nickel sulfide loading on decolorization process, three catalysts were prepared by ion exchange of zeolite P in 0.01, 0.1 and 0.2 M of  $\text{Ni}^{2+}$  solutions. Sulfonization of the samples was carried out according to above-mentioned method.

#### 2.4. Catalyst characterization

The X-ray diffraction patterns of zeolite P was performed using a Bruker diffractometer (D8 Advance) with Ni-filtered copper radiation ( $K_{\alpha} = 1.5406 \text{ \AA}$ ) and  $2\theta$  range of  $10\text{--}80^{\circ}$ . FT-IR spectra of the samples, on KBr pellets were recorded with a Nicolet single beam FT-IR (Impact 400D) spectrometer in the range of  $400\text{--}4000 \text{ cm}^{-1}$  at room temperature. Differential scanning calorimetry (DSC) and other thermograms (TG and DTG) were performed for the samples (6 mg) using Model Setaram STA units in the range of  $50\text{--}800^{\circ}\text{C}$  with temperature rise of  $10^{\circ}\text{C min}^{-1}$ .

#### 2.5. The catalytic activity

Photodecolorization experiments were performed with a photocatalytic reactor system. The bench-scale system is a cylindrical Pyrex-glass cell with 1.0L capacity, 10 cm inside diameter and 15 cm height. Irradiation experiments were performed using medium pressure Hg lamp (75 W), then it was placed in a 5 cm diameter quartz tube with one end tightly sealed by a Teflon stopper. The lamp and the tube were then immersed in the photoreactor cell with a light path of 3.0 cm. A magnetic stirrer was used continuously to guarantee good mixing of the solution. Unless otherwise stated, the reaction was carried out at room temperature under the conditions of  $0.8 \text{ g L}^{-1}$  of the solid catalyst in 50 mL solution of 20 ppm E.B.T. dye, and the pH of the solution was initially 5. Generally, HCl (1 M) and NaOH (1 M) were used to adjust the pH value in the beginning of all experiments including the effect of pH study. The decolorization of E.B.T. dye was analyzed by UV-vis spectrophotometer (Cary 100 Scan). The decolorization was determined at the wavelength of maximum absorption (525 nm) of the dye. In the investigation of pH, due to shift in the  $\lambda_{\text{max}}$  value, new  $\lambda_{\text{max}}$  was determined by scanning the samples in range of 300–800 nm. Decolorization efficiency was determined using absorbance of solutions before and after photodecolorization experiments. Calibration plots based on Beer's law were established with the absorbance and the concentration of dye. The decolorization of E.B.T. dye was fitted with first-order kinetics [ $\ln(C/C_0) = -kt$ ] (where  $C_0$  and  $C$  are the initial and final dye concentrations at time  $t$ , respectively, and  $k$ ,  $\text{min}^{-1}$ ), is the reaction rate constant). The rate constant,  $k$ , was calculated from the slopes of the straight-line portion of the plots [ $\ln(C/C_0)$  versus time]. To determine the surface adsorption amount, control experiments in the dark condition carried out in parallel in each case at the presence of catalyst on the decolorization of E.B.T.

### 3. Results and discussions

#### 3.1. XRD patterns

The X-ray diffraction (XRD) patterns of zeolite P (ZP), Ni-P, NiS-P and bulk NiS (the inset in Fig. 1) were shown in Figs. 1 and 2 in different  $2\theta$  ranges. The characteristic lines at  $2\theta$  ( $12.4$ ,  $17.8$ ,  $21.7$ ,  $28.2$  and  $33.3$ ) are observed from XRD pattern (curve a in Fig. 1) that shows a good agreement with the data of Na-P zeolite [27]. This analysis shows that the product has a typical zeolite P structure with no amorphous materials. Presence of the weak peaks in  $2\theta$  values of  $20^{\circ}$  and  $26.8^{\circ}$  in the Ni-P and NiS-P patterns (curves b and c in Figs. 1 and 2), that were not present in ZP pattern, can be

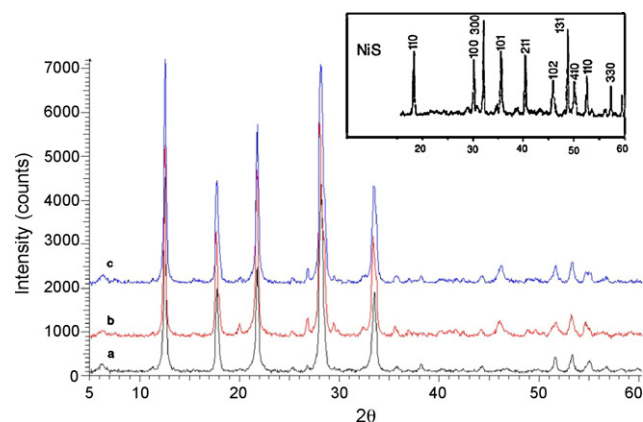


Fig. 1. X-ray diffraction pattern of parent synthesized zeolite P (a), Ni-P (b) and NiS-P (c) (in  $2\theta$  range of  $5\text{--}60^{\circ}$ ).

showed due to the incorporation of  $\text{Ni}^{2+}$  and Ni-S in the zeolite structure. The powder XRD results of the ZP and the host-guest composite materials, Ni-P and NiS-P (Figs. 1 and 2) show similar diffraction peaks indicative of zeolite P. But, some differences, such as the broadening of the diffraction peaks, increasing or decreasing of some peaks intensity as well as the shift of the peak position to the slightly lower angles can be observed in the spectra. In fact, the intensities of the peaks in the host-guest composite materials are increased with respect to those of zeolite P. This increase of the peak intensities, can be related to the presence or incorporation of semiconductor inside the matrix structure. These peaks are located approximately at  $2\theta$  equal to  $11.5^{\circ}$ ,  $18.8^{\circ}$ ,  $21.8^{\circ}$ ,  $28.2^{\circ}$  and  $33.5^{\circ}$  which are due to the reflection of the (1 0 0) and (3 0 0) planes, in the NiS phase [25]. Proceeding in the same way, we found an increase in intensity of some peaks in the case of NiS, at  $46^{\circ}$  and  $49^{\circ}$  which are related to the (1 0 2) and (4 1 0) planes of NiS phase [25]. Analysis of the  $\beta$ , excess width line of the diffraction peak in radians and  $\theta$ , the Bragg angle in degrees and by using the Debye-Scherrer formula,  $d = 0.9\lambda/\beta \cos\theta$ , where  $d$  is the average diameter of the crystal and  $\lambda$  the wavelength of X-ray, we determined the average size of ZP, bulk NiS and NiS-P to be 2.14, 1.52 and 1.90  $\mu\text{m}$ , respectively. The average diameter of the NiS incorporated in zeolite (extracted by HF digestion of NiS-P) was about 35 nm.

The crystallinity of the prepared samples were calculated using the ratio of the sum of the areas of the most intense peaks for samples (in above-mentioned  $2\theta$  values) to the same peaks for the zeolite P and multiplying by 100 and were obtained as 100, 101.8 and 103.9 for zeolite P, Ni-P and NiS-P, respectively. This indicate that zeolite structure do not change due to the incorporation of  $\text{Ni}^{2+}$  and NiS particles.

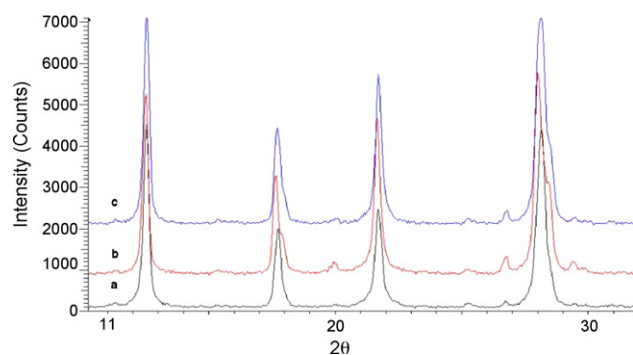


Fig. 2. X-ray diffraction pattern of parent synthesized zeolite P (a), Ni-P (b) and NiS-P (c) (in  $2\theta$  range of  $11\text{--}30^{\circ}$ ).

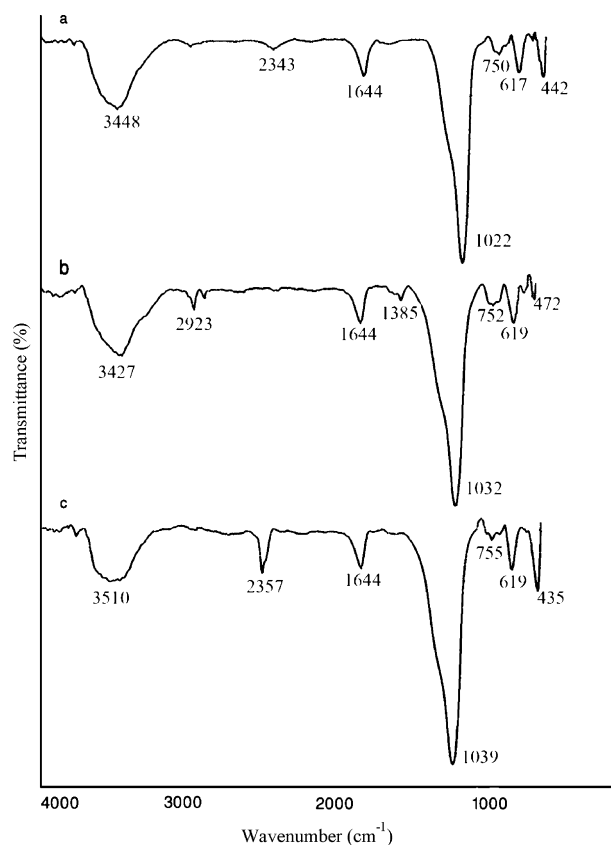


Fig. 3. FT-IR spectra of (a) Na-P, (b) Ni-P and (c) NiS-P zeolites.

### 3.2. FT-IR spectroscopy

FT-IR lattice vibration spectra were used to investigate the influence of nickel and nickel sulfide on the zeolite framework. Representative spectra of zeolite P, Ni-P and NiS-P in the range of 450–4000  $\text{cm}^{-1}$  are shown in Fig. 3. According to Fig. 3a, the observed frequencies at 3448, 1644, 1022, 750, 617 and 442  $\text{cm}^{-1}$  agrees with the infrared spectral data, which has been obtained for zeolite P by Flanigen et al. [28]. Infrared spectroscopy can reflect the change of the frameworks configuration of the zeolite host after the incorporation of the guests. Changes of the characteristic bands took place between the host zeolite P (the values in the parentheses) and the host-guest materials Ni-P and NiS-P. For Ni-P, the characteristic bands are seen at 472 (442)  $\text{cm}^{-1}$ , 619 (617)  $\text{cm}^{-1}$  (T-O bend), 533 (535)  $\text{cm}^{-1}$  (double rings) (the band between 617 and 750  $\text{cm}^{-1}$ ), 752 (750)  $\text{cm}^{-1}$  (symmetrical stretch), 1032 (1022)  $\text{cm}^{-1}$  (asymmetrical stretch) that show a shift of some bands as compared with the bands of the zeolite P host (Fig. 3a and b). The greenish blue color after ion exchange with  $\text{Ni}^{2+}$  ions is the primary evidence for incorporation of  $\text{Ni}^{2+}$  into zeolite framework. The similar results will be shown for NiS-P at 435, 619, 755 and 1039  $\text{cm}^{-1}$  (Fig. 3c). In addition, in NiS-P spectral changes around 755  $\text{cm}^{-1}$  are different from other spectra. These results demonstrated that the guest NiS incorporated into the zeolite P had some interactions with the inner surfaces of zeolite P host at the same time. The product after the precipitation process shows a change in color from greenish blue to pale gray that in turn can be shows conversion of  $\text{Ni}^{2+}$  to NiS in the zeolite.

### 3.3. Thermal analysis

The TG, DTG and DSC curves of zeolite P, Ni-P and NiS-P are shown in Fig. 4. According to DTG curves, water is lost in two steps

in zeolite P and NiS-P and three steps for Ni-P with a shoulder at 100 °C. The peaks at 100 and 152 °C (for zeolite P, Fig. 4a), 100, 159 and 200 °C (for Ni-P, Fig. 4b), 100 and 151 °C (for NiS-P, Fig. 4c) are seen in the DTG curves. This behavior is in accordance with the presence of two water sites (for zeolite P and NiS-P) and three water sites (for Ni-P) in the structure. Authors suggest that the elimination of the shoulder at the right side of the peak at NiS-P (with respect to Ni-P), indicates decrease in hydration of the structure due to precipitation of  $\text{Ni}^{2+}$  as NiS. The DTG results were confirmed by the data from the DSC curves which show an endothermic peak at 158, 166 and 157 °C for zeolite P, Ni-P and NiS-P, respectively. The peak at 328 °C (Fig. 4b) may be related to loss of nitrate that remained due to incomplete washing of the zeolite after ion exchange. Sulfur compounds must be evolved at 450–550 °C region [30]. Thermal curves of NiS-P show no evolve of any substances in this region. The obtained result shows the stability of NiS in the surface and cavity of the zeolite. The weight loss percent of ZP, Ni-P and NiS-P samples were obtained as 10.5, 14.9 and 10.5%, respectively. The second peak at 328 °C (Fig. 4b) for Ni-P sample which is related to loss of nitrate show 2.5% weight loss.

### 3.4. SEM analysis

The surface morphology of zeolite P (a–d), Ni-P (e) and NiS-P (f–h) has been studied by scanning electron microscopy and the SEM pictures of the unloaded zeolite and samples are presented in Fig. 5. The crystallites of the unloaded zeolite, with size about 1.75  $\mu\text{m}$ , have a very well defined spherical grain-like crystals. The image of the loaded samples also shows the spherical crystals that indicate the zeolite crystallites are not affected by the NiS loading. The average particle size of Ni-P and NiS-P samples is about 1.60 and 1.23  $\mu\text{m}$ , respectively. The image of loaded samples shows that spherical grain-like of zeolite crystals is not affected by the NiS and  $\text{Ni}^{2+}$  loading.

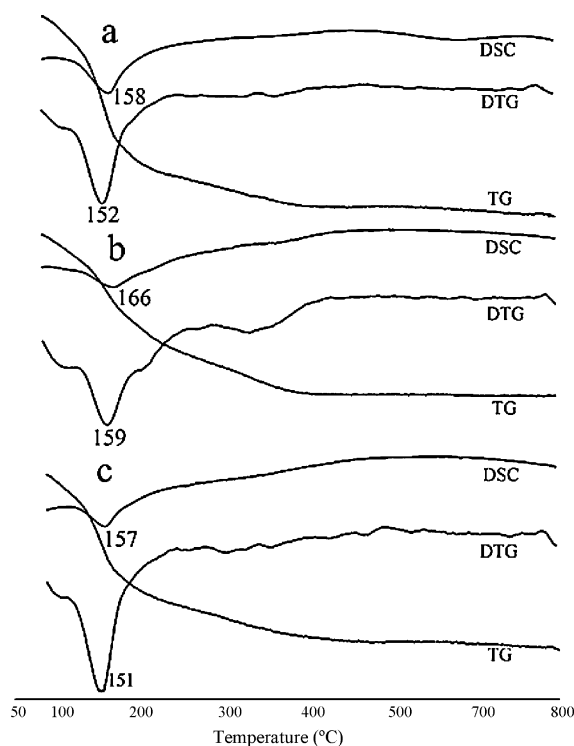


Fig. 4. Thermal analysis curves spectra of (a) Na-P, (b) Ni-P and (c) NiS-P zeolites.



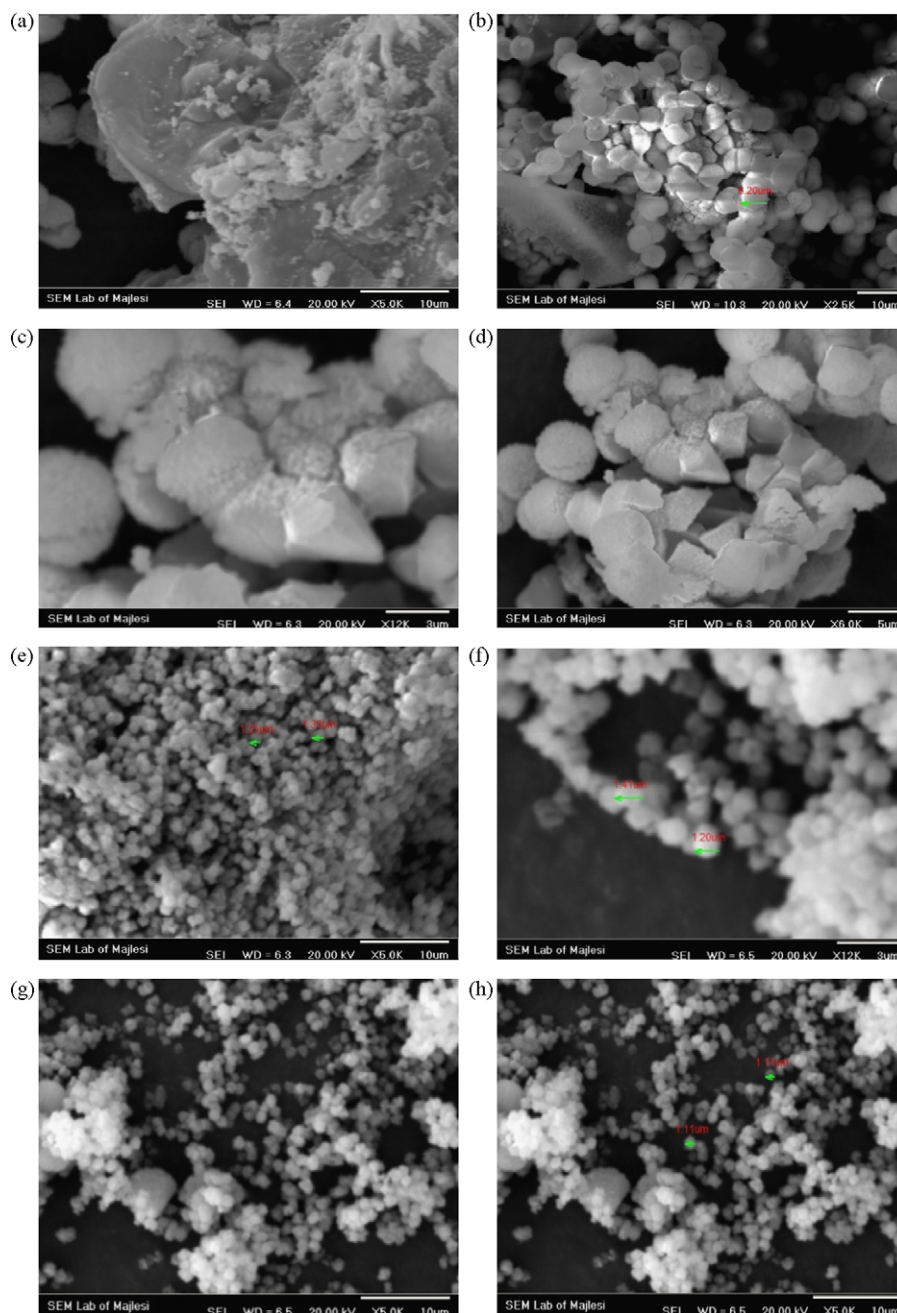


Fig. 5. SEM images of zeolite P (a–d), Ni–P (e) and NiS–P (f–h).

#### 4. Catalytic activity of NiS/zeolite P sample

##### 4.1. Effect of NiS loading

The influence of NiS loading on zeolite P on E.B.T. decolorization was studied using the same above-mentioned experimental conditions using  $0.5 \text{ g L}^{-1}$  of NiS–P catalyst. Three catalysts were prepared by ion exchange of zeolite P in 0.01, 0.1 and 0.2 M of  $\text{Ni}^{2+}$  solutions. According to atomic absorption result of nickel determination, their NiS contents were 2.1, 3.7 and 4.3%, respectively. Many authors reported that the kinetic behavior of photocatalytic reaction obey the first-order reaction [2,31]. In order to confirm the speculation,  $\ln(C/C_0)$  was plotted as a function of the irradiation time. The calculated results indicated that the first-order model gives a better fit. The rate constant values,  $k$  ( $\text{min}^{-1}$ ), are calculated

from the straight-line portion of the first-order plots as a function of the catalyst loading and are 0.0012, 0.0096 and  $0.0101 \text{ min}^{-1}$  for NiS loading of 2.1, 3.7 and 4.3%, respectively. As the results show, there is no significant difference between the decolorization efficiency of the catalyst containing 3.7 and 4.7% NiS. Hence, the optimum value of 3.7% NiS was used in later investigations.

##### 4.2. Effect of dosage of catalyst

The initial rate of photocatalytic decolorization of many pollutants is a function of the photocatalyst dosage [32]. The effect of the amount of NiS–P zeolite on E.B.T. dye decolorization efficiency versus time is presented in Fig. 6. It is seen that the decolorization rate increases with increasing mass of catalyst, reached the higher value ( $0.8 \text{ g L}^{-1}$  of the catalyst) and then decreased. The reason for

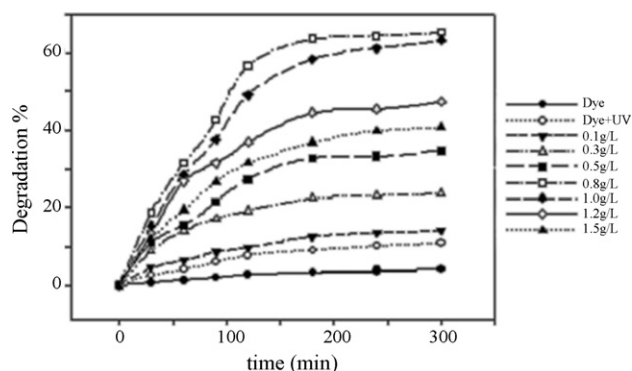


**Fig. 6.** Effect of NiS–P dosage on decolorization efficiency; initial dye concentration, 20 ppm; initial pH, 5.

this decrease is thought to be the fact that when the concentration of the catalyst rises, the solid particles increasingly block the penetration of the photons. So the overall number of the photons that can be reached to catalyst particles and the production of OH radicals are decreased with the loading of the catalyst [2]. Another reason may be due to the aggregation of solid particles while using large amount of catalyst was used [31]. Also, Fig. 4 shows the removal rates were negligible in the absence of catalyst or dark conditions. According to control experiment results, the surface adsorbed of E.B.T. has a 15% maximum value and this value was considered (decreased from total decolorization values) in all decolorization calculations.

In order to calculate  $k$  values,  $\ln(C/C_0)$  was plotted as a function of the irradiation time. The rate constant values,  $k$  ( $\text{min}^{-1}$ ), are calculated from the straight-line portion of the first-order plots as a function of the catalyst mass and are listed in Table 2. As the results show, maximum decolorization (63.5%) of E.B.T. dye was observed after 180 min with the maximum rate constant ( $7.7 \times 10^{-3} \text{ min}^{-1}$ ) in the presence of  $0.8 \text{ g L}^{-1}$  of the catalyst. Therefore,  $0.8 \text{ g L}^{-1}$  of the catalyst was used as optimum value.

#### 4.3. Effect of the initial dye concentration

Fig. 7 shows the effect of the initial concentration of dye on the decolorization efficiency versus time. The life time of hydroxyl radicals are very short (only a few nanoseconds) and thus they can only react where they are formed. Increasing the quantity of E.B.T. molecules per volume unit logically enhances the probability of collision between organic matter and oxidizing species, leading to an increase in the decolorization efficiency. It is seen that the decolorization efficiency of dye was decreased when increasing the initial concentration to more than 40 ppm. The decrease of decolorization percent with increase of dye concentration can be due to two reasons. With increasing amounts of dye, more of dye

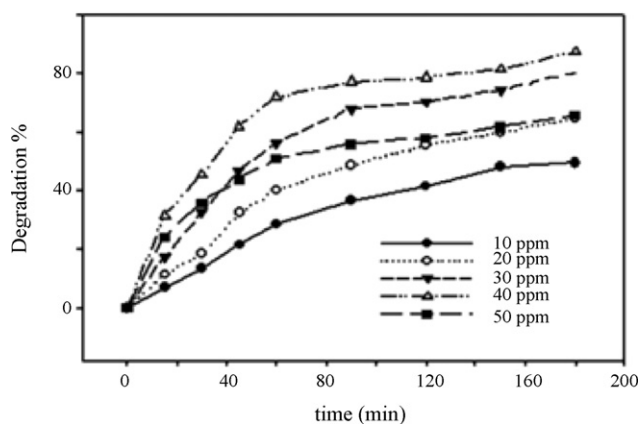


**Fig. 7.** Effect of the initial dye concentration on decolorization efficiency;  $0.8 \text{ g L}^{-1}$  of catalyst; initial solution pH, 5.

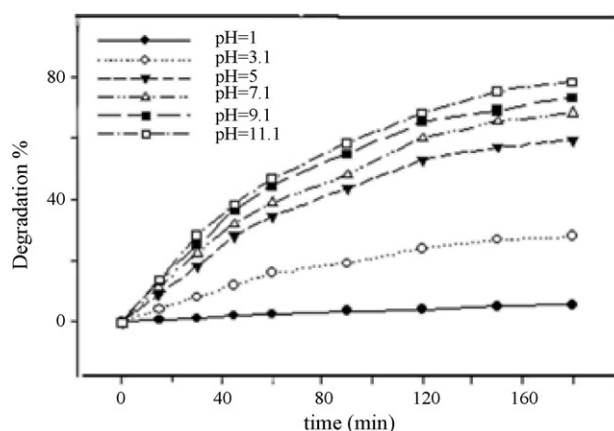


**Fig. 8.** Influence of solution pH on the E.B.T. dye decolorization;  $0.8 \text{ g L}^{-1}$  of catalyst; initial dye concentration, 20 ppm.

molecules will be adsorbed on the surface of the photocatalysts and the active sites of the catalysts will be reduced. Therefore, with increasing occupied space of catalyst surface, the generation of hydroxyl radicals will be decreased. Also, increasing concentration of dye can lead to decreasing number of photons that are arrived on the surface of catalysts. More light are absorbed by molecules of dye and the excitation of photocatalyst particles by photons will be reduced. These results are in good accordance with the literature [33]. This is also simplified in Table 3 where the decolorization rate constant ( $k$ ,  $\text{min}^{-1}$ ) is listed as a function of initial concentration of dye. It is apparent that the rate of decolorization is a quantitative of concentration dependent and the activity was increased with increasing concentration to 40 ppm.

#### 4.4. Influence of pH on the dye decolorization

The effect of solution pH in the range of 1–11 on E.B.T. dye decolorization efficiency versus time is presented in Fig. 8. The rate

**Table 2**  
Reaction rate constant of E.B.T. decolorization as a function of catalyst dosage.

Catalyst mass ( $\text{g L}^{-1}$ )	$\kappa$ $1000 \times (\text{min}^{-1})$
0 <sup>a</sup>	0.02
0 <sup>b</sup>	0.3
0.1	0.9
0.3	4.8
0.5	9.9
0.8	14.7
1.0	6.5
1.2	4.5
1.5	3.9

<sup>a</sup> 20 ppm dye under dark conditions.

<sup>b</sup> 20 ppm dye under UV irradiation conditions.

**Table 3**  
Reaction rate constant of E.B.T. decolorization as a function of the initial concentration of dyes.

$C_{\text{dye}}$ (ppm)	$\kappa$ $1000 \times (\text{min}^{-1})$
10	8.0
20	15.5
30	19.1
40	21.0
50	11.0

**Table 4**  
Reaction rate constant of E.B.T. decolorization as a function of initial solution pH.

pH	$\kappa$ 1000 $\times$ (min <sup>-1</sup> )
1.1	0.06
3.1	6.5
5	14.9
7.1	17.1
9.1	20.0
11.1	15.9

constant values ( $k$ , min<sup>-1</sup>) as a function of pH on the decolorization process are presented in Table 4. It is clear that the decolorization of the dye increases with raising pH. According to data of Table 4, it is apparent that the rate of decolorization is pH dependent and the activity is increased with increasing pH value. The maximum decolorization (78.5%) was achieved over NiS/P zeolite catalyst in 180 min at pH 9. As mentioned in the literature [2], in the initial acidic pHs, concomitant with acidification of the solution by HCl, a high amount of conjugated base is added to the solution. The anion Cl<sup>-</sup> is able to react with hydroxyl radicals leading to inorganic radical ions (ClO<sup>-•</sup>). These inorganic radical anions show a much lower reactivity than •OH, so that they do not take part in the dye decolorization. There is also a drastic competition between the dye and anions with respect to •OH. Hence, increase in pH shows an increase in decolorization efficiency. As the results show, there is a decrease in removal efficiency at pH higher than 9. Authors suggest that at high concentration of •OH two processes may take place leading to the deactivation of •OH. First, the H<sub>2</sub>O<sub>2</sub> and HO<sub>2</sub> radicals were formed due to the reaction of •OH with •OH. The reactivity of these radicals with organic dye is very low compared to that of •OH [2]. Second, due to the presence of high amounts of •OH radicals, the radical–radical reactions takes place at higher pH values. This reaction was reported in the literature [7]. Generally, the deactivation of •OH in high pH values was previously reported [2].

#### 4.5. Effect of the reaction temperature

The influence of temperature on the dye removal using 20 ppm dye concentration, pH 5 and 0.8 g L<sup>-1</sup> NiS/P zeolite was performed at 25, 50, 60 and 70 °C. Decolorization efficiency was increased by increasing temperature (Fig. 9). The rise in the temperature shows that it is effective at the initial stages of the process. Saïen et al. reported that an increase in temperature helps the reaction to compete more effectively with e<sub>cb</sub><sup>-</sup>–h<sub>vb</sub><sup>+</sup> recombination [34]. On the other hand, an increase in temperature decreases the solubility

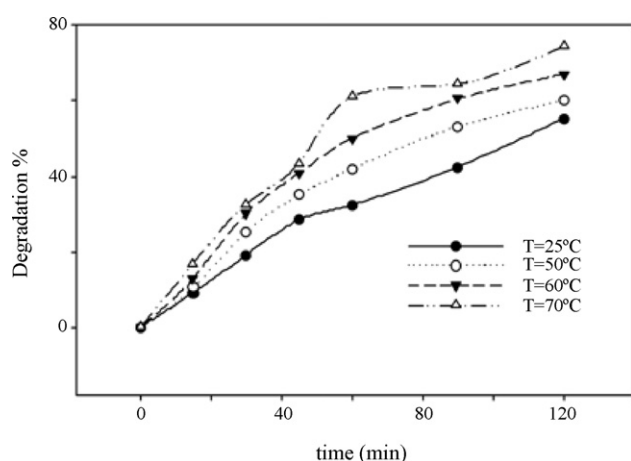


**Fig. 9.** Effect of the reaction temperature on degradation efficiency; 0.8 g L<sup>-1</sup> of catalyst; initial solution pH, 5; initial dye concentration, 20 ppm.

**Table 5**  
Reaction rate constant of E.B.T. decolorization as a function of reaction temperature.

Temperature (°C)	$\kappa$ 1000 $\times$ (min <sup>-1</sup> )
25	16.1
50	20.5
60	20.2
70	33.1

of oxygen in water which is not desirable. Higher temperatures will cause significant evaporation of the solution during the experiments. Thus, temperature higher than 50 °C not recommended. The rate constant values ( $k$ , min<sup>-1</sup>) as a function of temperature on the dye decolorization are presented in Table 5.

#### 4.6. Recovery experiments

The possibility of reusing the photocatalyst was examined to see the cost-effectiveness of the method. The catalyst was used in four consecutive experiments by using fresh dye solution at experimental conditions (20 ppm dye concentration, pH 5, 25 °C, 0.8 g L<sup>-1</sup> catalyst for 1 h). Between each experiment, the catalyst was removed by filtration and then washed with deionized water several times and dried at 90 and 240 °C for 2 h. As seen from Fig. 10, a small and gradual decrease in the activity of catalysts was observed at the first two cycles. But, decrease of the activity was seen intense after the first and second cycles for 90 °C drying temperature case. Decrease of the activity was not considerable for 240 °C drying temperature case. The decrease in activity of the used catalyst must reflect the presence of some adventitious decolorization products adsorbed in the zeolite, causing the partial blockage of the pore system or cover the zeolite surface. Preliminary thermal reactivation trials at 240 °C did lead to an appreciable decolorization of NiS–P photocatalyst as evidenced visually by the color change. Our results show a good agreement with the literature [33,35].

#### 4.7. Effect of zeolite

The amount of NiS loaded in zeolite measured by atomic absorption spectroscopy (by determination of Ni<sup>2+</sup>) was found to be 2.6 ppm. To determine whether the decolorization of E.B.T. by NiS takes place or not, the catalytic activity of 3 ppm NiS was measured under the same above-mentioned experimental conditions. No remarkable activity was noticed due to the presence of NiS as

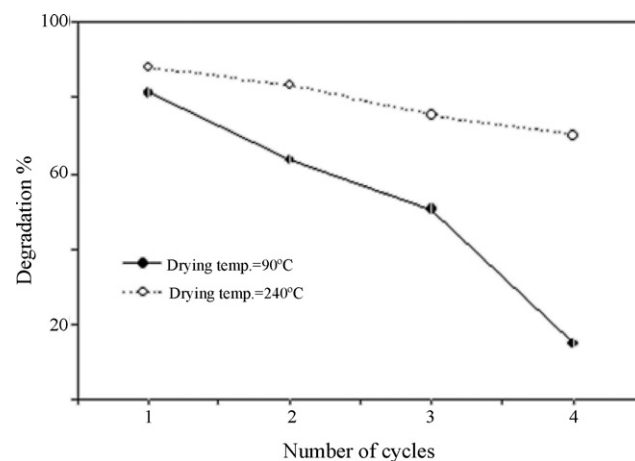


**Fig. 10.** Reproducibility of the catalyst for E.B.T. decolorization at 90 and 240 °C drying process; 0.8 g L<sup>-1</sup> of catalyst; initial solution pH, 5; initial dye concentration, 20 ppm.

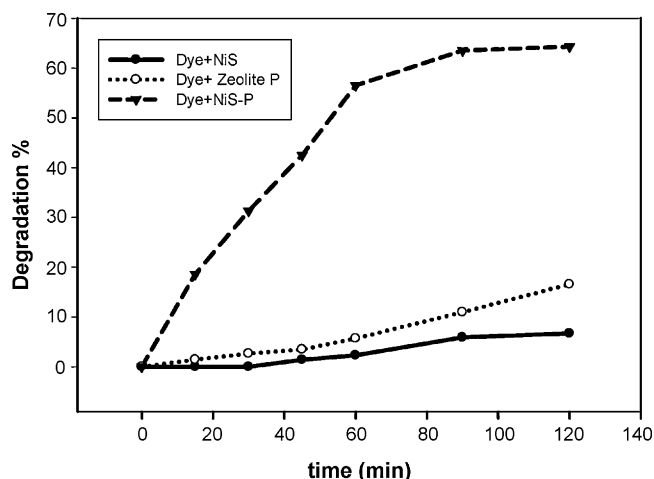


Fig. 11. Effect of zeolite on NiS photocatalytic activity.

shown in Fig. 11. It can be concluded that the decolorization process does not occur in the presence of NiS. The role of the zeolite might be correlated with the adsorption process, in the sense of high surface area and the decrease of particle size [31]. In our idea, in the absence of zeolite, NiS particles tend to aggregate that causes a decrease in active surface sites. But in the case of NiS incorporated zeolite, regarding to small and definite pore size of zeolite, there are small particles of NiS in the zeolite that increase available active sites of catalyst [35]. This in turn, causes an increase in photodecolorization efficiency. Catalytic efficiency of zeolite P toward E.B.T. decolorization was studied at above-mentioned conditions and the obtained results showed no considerable decolorization efficiency. These results also show that the responsible active centers for E.B.T. decolorization are NiS particles loaded on zeolite.

#### 4.8. UV-vis studies

Fig. 12 shows the decolorization of E.B.T. dye (20 ppm) under irradiation in time interval of 180 min and in the presence of NiS-P catalyst ( $0.8 \text{ g L}^{-1}$ , pH 5). The decrease of absorption spectra and therefore absorbance of samples at  $\lambda_{\text{max}}$  is indicated by decolorization of the dye in applied conditions. As a consequence the decrease of samples absorbance due to decrease of the dye concentration is recorded for measurement of decolorization rate in all above-mentioned parameters. Since there are no additional peaks appearing in the UV-vis spectra the dye is completely degraded. According to UV-vis spectra we suggest that product of the decolorization process are  $\text{H}_2\text{O}$ ,  $\text{CO}_2$ ,  $\text{NO}_2$  and  $\text{SO}_3$ . The pro-

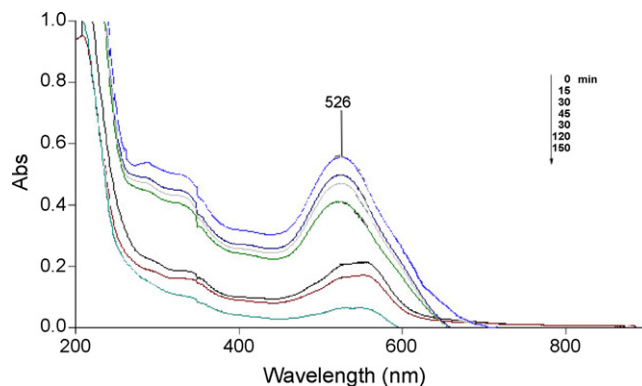


Fig. 12. Decrease absorption spectra of E.B.T. (20 ppm dye solution, pH 5) in the presence of NiS-P photocatalyst ( $0.8 \text{ g L}^{-1}$ ) in time interval of 180 min.

posed mechanism for dye decolorization using photocatalyst (PC) was suggested as follows:



## 5. Conclusions

The E.B.T. dye can be more efficiently degraded by NiS incorporated zeolite P in the presence of UV light. It is important to choose the optimal decolorization parameters for increasing the decolorization rate. The optimal operation parameters were found as follows: pH 9.1,  $0.8 \text{ g L}^{-1}$  of catalyst loading and 40 ppm of dye concentration. UV experiments showed a complete mineralization of E.B.T. The decolorization process obeyed first-order kinetics. The catalyst can be reused for dye decolorization with slightly less efficiency. Zeolite bed shows an important role in decolorization process so that NiS out of zeolite framework and zeolite P did not show significant decolorization efficiency. The results demonstrate that the active centers are NiS in the zeolite structure. SEM studies shows that the structure of zeolite crystals is not affected by the NiS and  $\text{Ni}^{2+}$  loading.

## References

- [1] H. Zollinger, Colour Chemistry: Synthesis Properties and Applications of Organic Dyes and Pigments, VCH Publishers, New York, 1991.
- [2] M.B. Kasiri, H. Aleboeyeh, A. Aleboeyeh, Decolorization of acid blue 74 using Fe-ZSM5 zeolite as a heterogeneous photo-Fenton catalyst. Appl. Catal. B: Environ. 84 (2008) 9–15.
- [3] C. Guillard, H. Lachheb, A. Houas, M. Ksibi, E. Elaloui, J.-H. Herrmann, Influence of chemical structure of dyes, of pH and of inorganic salts on their photocatalytic decolorization by  $\text{TiO}_2$ : comparison of the efficiency of powder and supported  $\text{TiO}_2$ . J. Photochem. Photobiol. A: Chem. 158 (2003) 27–36.
- [4] M.M. Nassar, H.Y. Magdy, Removal of different basic dyes from aqueous solutions by adsorption on palm-fruit bunch particles, Chem. Eng. J. 66 (1997) 223–226.
- [5] M. Boeningo, Carcinogenicity and Metabolism of Azodyes Especially Those Derived From Benzidine. DNHS (NIOSH) publication 80–119, U.S. Government Printing Office, Washington, DC, 1994 (July), pp. 80–119.
- [6] S. Anandan, M. Yoon, Photocatalytic activities of the nano-sized  $\text{TiO}_2$ -supported Y-zeolites. J. Photochem. Photobiol. C: Photochem. Rev. 4 (2003) 5–18.
- [7] S. Ashraf, M.A. Rauf, S. Alhadrami, Decolorization of methyl red using Fenton's reagent and the effect of various salts, Dyes Pigments 69 (2006) 74–78.
- [8] C. Zhu, L. Wang, L. Kong, X. Yang, L. Wang, S. Zheng, F. Chen, F. MaiZhi, H. Zong, Photocatalytic decolorization of AZO dyes by supported  $\text{TiO}_2$ /UV in aqueous solution, Chemosphere 41 (2000) 303–309.
- [9] I.T. Peternal, N. Koprivanac, A.M.L. Bozic, H.M. Kusic, Comparative study of UV/ $\text{TiO}_2$ , UV/ $\text{ZnO}$  and photo-Fenton processes for the organic reactive dye decolorization in aqueous solution, J. Hazard. Mater. 148 (2007) 477–484.
- [10] C.F. Patterson, Industrial Wastewater Control, Academic Press, USA, 1991.
- [11] U. Rott, R. Minke, Overview of wastewater treatment and recycling in the textile processing industry, Water Sci. Technol. 40 (1) (1999) 137–144.
- [12] Z. Aksu, Application of biosorption for the removal of organic pollutants: a review, Process Biochem. 40 (2005) 997–1026.
- [13] E. Forgacs, T. Cserhatia, G. Oros, Removal of synthetic dyes from wastewaters: a review, Environ. Int. 30 (2004) 953–971.
- [14] S. Parsons, Advanced Oxidation Processes for Water and Wastewater Treatment, IWA, London, 2004.
- [15] S. Ledakowicz, M. Solecka, R. Zylla, Biodecolorization, decolourisation and detoxification of textile wastewater enhanced by advanced oxidation processes, J. Biotechnol. 89 (2001) 175–184.
- [16] M. Pera-Titus, V. Garcia-Molina, M.A. Baos, J. Giménez, S. Esplugas, Decolorization of chlorophenols by means of advanced oxidation processes: a general review, Appl. Catal. B: Environ. 47 (2004) 219–256.



- [17] T. Oppenlander, Photochemical Purification of Water and Air, WILEY-VCH Verlag, 2003.
- [18] M. Tekbas, H.C. Yatmaz, N. Bektaş, Heterogeneous photo-Fenton oxidation of reactive azo dye solutions using iron exchanged zeolite as catalyst, *Micropor. Mesopor. Mater.* 115 (2008) 594–602.
- [19] A. Aleboyeh, H. Aleboyeh, Y. Moussa, Critical effect of hydrogen peroxide in photochemical oxidative decolorization of dyes: acid Orange 8 Acid Blue 74 and Methyl Orange Dyes and Pigments, vol. 57, 2003, pp. 67–75.
- [20] P.R. Gogate, A.B. Pandit, A review of imperative technologies for wastewater treatment. II. Hybrid methods, *Adv. Environ. Res.* 8 (2004) 553–597.
- [21] F.I. Hai, K. Yamamoto, K. Fukushi, Hybrid treatment systems for dye wastewater, *Crit. Rev. Env. Sci. Technol.* 37 (2007) 315–377.
- [22] M.A. Gondal, M.N. Sayeed, A. Alarfai, Activity comparison of  $\text{Fe}_2\text{O}_3$ ,  $\text{NiO}$ ,  $\text{WO}_3$ ,  $\text{TiO}_2$  semiconductor catalysts in phenol decolorization by laser enhanced photo-catalytic process, *Chem. Phys.* 445 (2007) 325–330.
- [23] M.C. Dalconi, A. Alberti, G. Cruciani, P. Ciambelli, E. Founda, Siting and coordination of cobalt in ferrierite: XRD and EXAFS studies at different Co loadings, *Micropor. Mesopor. Mater.* 62 (2003) 191–209.
- [24] I. Othman, R. Mohamady, I.A. Ibraheem, M.M. Mohamed, Synthesis and modification of ZSM-5 with manganese and lanthanum and their effects on decolorization of indigo carmine dye, *Appl. Catal. A* 299 (2006) 95–102.
- [25] Sh. Sohrabnezhad, A. Pourahmad, M.S. Sadjadi, M.A. Zanjanchi, Growth and characterization of NiS and NiCoS nanoparticles in mordenite zeolite host, *Mat. Sci. Eng.: C* 28 (2008) 202–205.
- [26] D.Q. Wang, D.R. Chen, X.L. Jiao, Synthesis of nickel sulfide particles by solvothermal process, *Chin. Chem. Lett.* 15 (2004) 79–82.
- [27] H. Faghihian, M. Kamali, Synthesis of Na-P zeolite from perlite and study of its ability to remove cyanide from liquid wastes, *Int. J. Environ. Pollut.* 19 (6) (2003) 557–566.
- [28] E.M. Flanigen, H. Khatami, H.A. Szymanski, *Molecular Sieve Zeolites Advances in Chemistry Series*, vol. 101, American Chemical Society, Washington, D.C., 1971, pp. 201.
- [29] A. Moirou, A. Vaxevanidou, G.E. Christidis, A.I. Paspaliaris, Ion exchange of zeolite Na-P with  $\text{Pb}^{2+}$ ,  $\text{Zn}^{2+}$  and  $\text{Ni}^{2+}$  ions, *Clays Clay Miner.* 48 (5) (2000) 563–571.
- [30] D.A. Skoog, J.J. Leary, *Principles of Instrumental Analysis*, 4th ed., Saunders College Publishing, New York, 1992, pp. 574–575.
- [31] Z.M. El-Bahy, M.M. Mohamed, F.I. Zidan, M.S. Thabet, Photo-decolorization of acid green dye over Co-ZSM-5 catalysts prepared by incipient wetness impregnation technique, *J. Hazard. Mater.* 153 (2008) 364–371.
- [32] M.S.T. Goncalves, A.M.F. Oliveria-campos, E.M.M.S. Pinto, P.M.S. Plasencia, M.J.R.P. Queiros, Photochemical treatment of solutions of azo dyes containing  $\text{TiO}_2$ , *Chemosphere* 39 (1999) 781–786.
- [33] H.R. Pouretedal, A. Norozi, M.H. Keshavarz, A. Semnani, Nanoparticles of zinc sulfide doped with manganese, nickel and copper as nanophocatalyt in the decolorization of organic dyes, *J. Hazard. Mater.* 162 (2009) 674–681.
- [34] J. Saien, A.R. Soleymani, Decolorization and mineralization of direct blue 71 in a circulating upflow reactor by UV/ $\text{TiO}_2$  process and employing a new method in kinetic study, *J. Hazard. Mater.* 144 (2007) 506–512.
- [35] M. Alvaro, E. Carbonell, M. Esplá, H. Garcia, Iron phthalocyanine supported on silica or encapsulated inside zeolite Y as solid photocatalysts for the decolorization of phenols and sulfur heterocycles, *Appl. Catal. B: Environ.* 57 (2005) 37–42.